Phytochemical Characterization, Functional Nutrition, and Anti-Diabetic Potentials of *Leptadenia hastata* (pers) Decne Leaves: In Silico and In Vitro Studies

Bioinformatics and Biology Insights
Volume 16: 1–17

DOI: 10.1177/11779322221115436
SAGE

Ifeoma Felicia Chukwuma[1,2], Florence Nkechi Nworah[1], Victor Onukwube Apeh[3], Kingsley Ozioma Omeje[1], Ekene John Nweze[1], Chukwudi Daniel Asogwa[1] and Timothy Prince Chidike Ezeorba[1,2,4]

[1]Department of Biochemistry, Faculty of Biological Sciences, University of Nigeria, Nsukka, Nigeria. [2]Department of Genetics and Biotechnology, Faculty of Biological Sciences, University of Nigeria, Nsukka, Nigeria. [3]Department of Applied Sciences, Federal College of Dental Technology and Therapy, Enugu, Nigeria. [4]Department of Molecular Biotechnology, School of Biosciences, University of Birmingham, Birmingham, UK.

ABSTRACT: The geometrical increase in diabetes mellitus (DM) and the undesirable side effects of synthetic drugs have intensified efforts to search for an effective and safe anti-diabetic therapy. This study aimed to identify the antioxidant and anti-diabetic agents in the ethanol extract of *Leptadenia hastata* (EELH). The phytochemicals, antioxidant vitamins, and minerals present in EELH were determined using standard procedures to achieve this aim. Gas chromatography coupled with mass spectroscopy and flame ionization detector (GC-MS/GC-FID) was employed to identify bioactive compounds. An e-pharmacophore model was generated from the extra precision, and energy-minimized docked position of standard inhibitor, acarbose onto human pancreatic amylase (HPA, PDB-6OCN). It was used to screen the GC-MS/GC-FID library of compounds. The top-scoring compounds were subjected to glide XP-docking and prime MM-GBSA calculation with the Schrodinger suite-v12.4. The Adsorption, Distribution, Metabolism, Excretion, and Toxicity (ADMET) prediction of the best-fit compounds was made using SwissADME and PROTOX-II webservers. Further validation of the docking results was performed with the in vitro analysis of the α-amylase and α-glucosidase inhibitory activities. EELH contains appreciable amounts of antioxidant and anti-diabetic phytoconstituents. The top-4 scoring compounds (rutin, epicatechin, kaempferol, and naringenin) from the EELH phytochemical library interacted with amino acid residues within and around the HPA active site. The ADMET prediction shows that epicatechin, kaempferol, and naringenin had favorable drug-likeness, pharmacokinetic properties, and a good safety profile. EELH demonstrated good inhibitory actions against α-amylase and α-glucosidase with $1C_{50}$ values of 14.14 and 4.22 µg/mL, respectively. Thus, *L hastata* phytoconstituents are promising novel candidates for developing an anti-diabetic drug.

KEYWORDS: ADMET, diabetes mellitus, human pancreatic amylase, ***Leptadenia hastata***, molecular docking, pharmacophore modeling

RECEIVED: April 21, 2022. **ACCEPTED:** July 4, 2022.

TYPE: Original Research Article

FUNDING: The author(s) received no financial support for the research, authorship, and/or publication of this article.

DECLARATION OF CONFLICTING INTERESTS: The author(s) declared no potential conflicts of interest with respect to the research, authorship, and/or publication of this article.

CORRESPONDING AUTHOR: Timothy Prince Chidike Ezeorba, Department of Biochemistry, Faculty of Biological Sciences, University of Nigeria, Nsukka 410001, Enugu State, Nigeria. Email: timothy.ezeorba@unn.edu.ng

Introduction

Diabetes mellitus (DM) is a metabolic endocrine disorder affecting carbohydrates, proteins, and lipid metabolism,[1,2] with a mortality rate of 4.9 million people worldwide,[3,4] which is higher than the death rate of 1.5 million (tuberculosis), 1.5 million (human immunodeficiency virus), and 0.6 million (malaria), combined.[5] The derangement in carbohydrate metabolism could impair insulin secretion, insulin action, or both.[6,7] Although all forms of DM have hyperglycemia (fasting blood glucose ⩾ 126 mg/dL) in common, the cause and clinical manifestations vary widely. The American Diabetes Association classified diabetes into 2 major categories: Type 1 diabetes (T1D), caused by autoimmune destruction of the β-cell of the pancreas by producing specific antibodies against its cells,[1] and type 2 diabetes (T2D) as a result of a combination of resistance to insulin action and a secretory response by pancreatic β-cells that is inadequate to overcome insulin resistance, leading to relative insulin deficiency.[4] According to WHO data, more than 250 million people are currently living with diabetes, with this figure anticipated to rise to more than 592 million by 2035,[8] with T2D accounting for 80% to 90% of DM.[3,4] Astonishingly, a more significant percentage of people with DM are unaware that they have hyperglycemia until it gets to long-term hyperglycemia.[9]

Long-term hyperglycemia elicits macrovascular (large- and medium-sized muscular arteries) and microvascular (small vessel) complications, leading to diabetic retinopathy, nephropathy, neuropathy, polyurea, polyphagia, and atherosclerosis, which are the significant causes of morbidity and mortality worldwide.[2,10] Management/treatment options for DM range from lifestyle modification, exercise, insulin injection, and use of anti-DM drugs.[5,11] The biochemical basis of most anti-DM drugs involves inhibiting the catalytic activities of carbohydrate metabolizing enzymes, such as human pancreatic α-amylase (HPA) and α-glucosidase, which reduces blood sugar levels by suppressing carbohydrate digestion and glucose uptake,[3,8] making them the primary targets in controlling blood glucose in DM patients.[12-14] Studies have shown that inhibition of

HPA is a better suppressor of postprandial hyperglycemia (PPHG) than α-glucosidase because it prevents excessive accumulation of maltose.[13]

Human pancreatic α-amylase (EC:3.2.1.1) hydrolyzes carbohydrates and starch to oligosaccharides (maltose, maltotriose, and limit dextrin) by cleaving endo α-(1,4) glycosidic linkages.[15] Hence, inhibition of HPA, which controls PPHG, is the major therapeutic target in managing/treating T2D. Acarbose is a conventional anti-DM drug, mostly prescribed as an HPA inhibitor. Although it is effective as an anti-DM agent, prolonged usage could result in detrimental side effects, such as sudden hypoglycemia, diarrhea, weight gain, unusual bleeding, allergic reactions, and anorexia.[13] To address the challenges of contraindications, significant side effects, high cost, and limited therapeutic effects of synthetic drugs, the WHO expert committee on DM has recommended evaluating herbal remedies currently employed in managing diabetes.[2] Consequently, screening and isolation of anti-diabetic agents from plant-based phytochemicals is gaining momentum globally,[16] due to their proven efficacy, attractive, and holistic drug action with better safety profile.[6,13,17–19] Phytochemicals in plants, such as flavonoids, tannins, and phenols, avert the onset of long-term diseases including DM by scavenging free radicals, thereby restoring cellular damage caused by redox equilibrium disruption.[18,20-23]

Leptadenia hastata (pers.) Decne, a member of the *Asclepiadaceae* family widely distributed in Tropical Africa, is one of the herbal remedies used by traditional healers to treat DM.[11,24] Furthermore, several experimental studies have reported the anti-diabetic activity of *L hastata*.[7,11,17] Other reported pharmacological and biological potentials of different parts of *L hastata* include antimicrobial, antiandrogenic, anti-inflammatory, and antibacterial activities.[24] The anti-DM activity of medicinal plants is also anchored on active pharmaceutical phytoconstituents, including phytochemicals, vitamins, and minerals.[11] This study investigated the phytochemicals, vitamins, and minerals in *L hastata* and employed computational techniques to discover potential HPA antagonists, drug-likeness, pharmacokinetics properties, and safety profiles of compounds identified in ethanol extract of *L hastata* (EELH) using gas chromatography–mass spectrophotometer (GC-MS) and gas chromatography–flame ionization detector (GC-FID). Furthermore, inhibition of α-amylase and α-glucosidase was used to validate the anti-DM of the plant.

Materials and Methods

Plant collection and identification

Fresh leaves of *L hastata* were obtained from the University of Nigeria Botanical Garden, Enugu State, Nigeria (Latitude: 6.8645°N, Longitude: 7.4083°E). The plant was identified and authenticated by Mr Alfred Ozioko, a Taxonomist at Bioresources Development and Conservation Program (BDCP) Research Center Nsukka, Enugu state. The plant leaf samples were also deposited in the Herbarium (Voucher No./INTERCEDD/503) for reference purposes.

Chemicals/reagents. Analytical grade chemicals used for the study were procured from the following reputable companies: ammonia solution, ethyl acetate, dinitrosalicylic acid, ferric chloride, sodium carbonate, and sucrose were procured from British Drug Houses (BDH) chemicals Ltd, Poole, England; α-amylase (EC:3.2.1.1), α-glucosidase (EC:3.2.1.20), ethanol, chloroform, folin-ciocalteau reagent, glacial acetic acid, sulfuric acid, and Wagner reagents were sourced from Sigma-Aldrich Inc, UK. While distilled/deionized water obtained from the National Center for Research and Development, University of Nigeria, Nsukka was used to prepare chemicals and reagents.

Preparation of the extract

The extract was prepared using 417 g of dry ground sample and 1000 mL of an absolute ethanol solution by cold maceration at room temperature. The mixture was shaken intermittently at room temperature for 72 hours and filtered through Whatman filter paper number 1 (pore size 11 m). The final extract was concentrated on a rotatory vacuum evaporator (R-215, Buchi, Flawil, Switzerland) at 45°C and under reduced pressure. The dried extract was kept in a refrigerator at −4°C till used in the experiment.

Qualitative phytochemical screening

Qualitative phytochemical screening of EELH was carried out to determine the presence of alkaloids, flavonoids, tannins, saponins, cardiac glycosides, terpenoids, and steroids using standard methods of previous studies[25–27] as follows.

Alkaloids: Alkaloids were qualified in the extract by boiling (0.5 g) with 6 mL aqueous HCl (1%). The formation of a reddish-brown precipitate (ppt) after adding 2 drops of Wagner's reagent to the filtrate indicated the presence of alkaloids.

Flavonoids: The presence of flavonoids in the extract was qualified by boiling 0.1 g of the extract in 10 mL ethyl acetate for 3 minutes. Then, 4 mL of the cooled filtrate was shaken with a dilute ammonia solution (1 mL). An intense yellow ppt indicated the presence of flavonoids.

Tannins: A quantity (0.1 g) of the extract was added to deionized water (10 mL) and filtered before adding ferric chloride (3 drops). The formation of a greenish-brown ppt confirmed the presence of tannins.

Saponins: The extract (0.1 g) was added to deionized water (200 mL) and shaken vigorously for 15 minutes. The formation of the foam layer indicated the presence of saponins.

Cardiac glycosides: Few drops of ferric chloride (5%) and glacial acetic acid (2 mL) were added to 0.1 g of the extract, forming the brown ring at the interface after adding concentrated sulfuric acid (1 mL) confirmed the presence of cardiac glycosides.

Terpenoids: Chloroform (2 mL) was added to 0.1 g of the extract in a test tube. The formation of reddish-brown color confirmed the presence of terpenoids at the interface after adding concentrated sulfuric acid (1.5 mL).

Steroids: To 0.1 g of the extract, chloroform (2 mL) and sulfuric acid (1 mL) were added. The formation of a reddish-brown ring at the interface indicated the presence of steroids.

Determination of antioxidant vitamins

Vitamins A, C, and E were determined using the spectrophotometer technique according to the procedures of the Association of Vitamin Chemists[28] as follows.

Vitamin A. The procedure involves the precipitation of the sample (2 g) with 3 mL of absolute ethanol followed by the extraction of vitamin A with 5 mL of heptane. The mixture obtained was vigorously shaken for 5 minutes and allowed to separate into layers. After that, the heptane layer (3 mL) was used to quantify the vitamin A content at a wavelength of 450 against a blank of heptane. The concentration of vitamin A was obtained from the standard curve.

Vitamin C. The vitamin C content of the extract was determined by titration with diphenol indo 2, 6-dichlorophenol (DPIP). The sample (0.2 g) was added to a test tube containing 4 mL of buffer solution (1 g/L oxalic acid and 4 g/L sodium acetate anhydrous). The resulting solution was DPIP (295 mg/L) and sodium bicarbonate (100 mg/L). The content of vitamin C in the seeds was calculated from equation (5) below

$$\text{Vitamin C}\left(\text{mg}/100\ \text{g}\right)=\frac{\text{MV}\times 100\times 100}{10\text{B}}$$

where M is the mass of ascorbic acid titrimetric equivalent to 0.001 M DPIP solution (mg); 100 is the dilution ratio of the sample taken; the second 100 is the scaling factor for conversion to per 100 g of raw material, and 10 is the titrate volume; V is the titrant volume (0.001 M DPIP solution) mL; and B is the weight of the sample extract used.

Vitamin E. The sample (1 g) was macerated in 20 mL of n-hexane. After that, the mixture was centrifuged for 10 minutes at 1500 rpm (4000 rpm, Abman, Canada), filtered, and treated with ethanol and alcoholic potassium hydroxide (0.5 N). Subsequently, 2 mL of the filtrate was evaporated to dryness in a boiling water bath (Gallenkamp, England). The residue was mixed with ethanol, ferric chloride (0.2%), and a-a 1-dipyridyl (0.5%). The absorbance of the resulting solution was taken against blank at 520 nm, and the concentration of vitamin E was calculated from the equation below

$$\text{Vitamin E}\ \left(\text{Mg}/100\ \text{g}\right)=\frac{\textit{Absorbance of sample}\times \textit{Conc. of standard}}{\textit{Absorbance of standard}}$$

Determination of mineral content

The mineral contents (calcium, manganese, zinc, copper, and iron) of the extract were measured with an atomic absorption spectrophotometer (AAS) Model AA-7000 (Shimadzu, Japan) according to the method of AOAC.[29] Each mineral was analyzed using its respective wavelength, after which its concentration was generated from the standard graph and expressed in ppm.

Screening of chemical compounds

The GC-MS analysis of compounds from the extract was determined using an Agilent Technologies GC system with the GC-M910 model (Buck Scientific, Santa Clara, CA, USA) equipped with an HP-5MS column (30 m in length, 250 m in diameter, and 0.25 m in thickness of film). Spectroscopic detection by GC-MS involved an electron ionization system that used high-energy electrons (70 eV). Pure helium gas (99.995%) was used as the carrier gas with a flow rate of 1 mL/min. The initial temperature was set at 50°C to 150°C with an increasing rate of 3°C/min and a holding time of about 10 minutes. Finally, the temperature was increased to 300°C at a rate of 10°C/min. Therefore, 1 µL of the prepared 1% extracts diluted with respective solvents was injected in a splitless mode. The relative quantity of the volatile compounds present in the EELH was expressed as a percentage based on the peak area produced in the chromatogram. Compounds were identified based on GC retention time (RT) on the HP-5MS column and matching the spectra with computer software standards (Replib and Mainlab data of GC-MS systems).

The BUCK M910 GC equipped with an FID was also employed to analyze phytochemicals according to the procedure of Bezerra and Filho.[30] In quantitative analysis, 150 µL of betulin solution was added to each vial before derivatization. It was performed on a RESTEK 15-m MXT-1 column (15 m × 250 µm × 0.15 µm). The injector temperature was 280°C with a splitless injection of 2 µL of sample and a linear velocity of 30 cm/s; Helium 5.0 Pa.s was the carrier gas with a flow rate of 40 mL/min. The oven operated initially at 200°C. It was heated to 330°C at a rate of 3°C/min and was kept at this temperature for 5 minutes. The detector operated at a temperature of 320°C. Phytochemicals were determined by the ratio between the area and mass of the internal standard and the area of the identified phytochemicals. The concentration of the different phytochemicals was expressed in µg/g.

Retrieval and preparation of crystal protein structure

The X-ray crystallography structure of the HPA co-crystallized with Montbretin. An analog was retrieved from the Protein Data Bank (PDB ID: 6OCN). The structure's quality and high resolution (1.147 Å) influenced our decision to use it.[31] The retrieved structure was prepared using the protein

preparation wizard of the Schrodinger suite v12.4 to obtain a final processed structure by assigning bond orders, the addition of missing hydrogens, simulation of disulfide bonds, conversion of selenomethionine to methionine, filling up missing side chains and loops, removal of water molecules beyond 5 Å, and finally minimizing the restrained energy of the structure. The quality of the preprocessed structure was assessed by the protein reliability report and Ramachandran plot (Supplementary Figure 1).

Preparation of ligand's library

The ligand library used for this study was prepared and curated from the *L hastata* class of phytochemical compounds obtained from the GC-MS analysis. The canonical SMILES representation of the structures of the curated compounds was retrieved from PubChem (https://pubchem.ncbi.nlm.nih.gov/) and using the LigPrep tools of Schrodinger suite v12.03; the 3D energy-minimized structure of the compounds were obtained and used for the pharmacophore and docking experiments.

Binding site predictions and grid generation for molecular docking

Pockets with a high likelihood of binding small molecules and phytoconstituents of EELH were predicted using the sitemap tools of Schrodinger suite v12.03. The best binding site was selected based on the site score and volume (Supplementary Table 1). The docking grid (as represented in Supplementary Figure 3) was generated around the most probable binding site. It was used for the docking standard drugs (Acarbose, Supplementary Figure 4) and compounds with probable bioactivities as screened from the pharmacophore model.

Generating an e-pharmacophore model for ligand library screening

The e-pharmacophore model was generated using the complex of the prepared crystal structure of HPA and a US Food and Drug Administration (FDA)-approved standard inhibitor against HPA (acarbose). The energy-minimized structure of acarbose, retrieved from PubChem and prepared using the LigPrep program of Schrodinger suite v12.4, was docked using the induced-fit docking (IFD) module of the same program onto the prepared crystal structure of HPA (ID: 6OCN). The best docking pose, determined from the docking score, was used to generate the e-pharmacophore model of the protein-ligand complex on the phase module of the Schrodinger suite v12.4. The phase module was programmed to provide a standard set of 6 pharmacophore features, namely hydrogen bond acceptor (A), hydrogen bond donor (D), hydrophobic group (H), negatively ionizable (N), positively ionizable region (P), and aromatic ring (R). As reported in Kikiowo et al,[32] the vectorial properties of those features are the hydrogen bond acceptor (A) and donor (D) as they determine the direction of electron sharing. In our study, the phase program was set to 7 features. However, our e-pharmacophore hypothesis generated only 5 features, which were used to screen the library of EELH compounds. Compounds from the library with a fitness greater than 1 and at least 3 of 5 pharmacophoric features were selected for molecular docking experiments.

Molecular docking experiments

Molecular docking predicts the most viable orientation of ligands in the binding pockets of receptors allotting scoring to their complex based on the strength of the interactions. About 7 compounds screened from the ligand library using the pharmacophore model were docked onto the prepared crystal structure of HPA (ID-6OCN) using both standard precision (SP-GLIDE) and extra precision (X-GLIDE). The interaction for hit compounds (selected based on the X-glide score) was further examined for their 2D and 3D interaction.

Binding free energy calculation

The binding free energy (ΔG_{bind}) of the hit compounds to the crystallized protein (6OCN) was calculated using the molecular mechanics–generalized Born surface area (MM-GBSA) model of the Prime Package of Schrodinger v12.4. The OPLS3 force field and VSGB solvation model were adopted for the ΔG_{bind} calculation. The MM-GBSA model estimated the ΔG_{bind} according to the following equation

$$\Delta Gbind = \Delta E + \Delta G_{solv} + \Delta G_{SA} \quad (1)$$

$$\Delta E = E_{complex} - E_{protein} - E_{ligand} \quad (2)$$

where $E_{complex}$, $E_{protein}$, and E_{ligand} are the minimized energies of the protein-inhibitor complex, protein, and inhibitor, respectively

$$\Delta G_{solv} = G_{solv(complex)} - G_{solv(protein)} - Gsolv_{(ligand)} \quad (3)$$

where $G_{solv(complex)}$, $G_{solv(protein)}$, and $G_{solv(ligand)}$ are the solvation free energies of the complex, protein, and inhibitor, respectively

$$\Delta G_{SA} = G_{SA(complex)} - G_{SA(protein)} - G_{SA(ligand)} \quad (4)$$

where $G_{SA(complex)}$, $G_{SA(protein)}$, and $G_{SA(ligand)}$ are the surface area energies for the complex, protein, and inhibitor, respectively.

ADMET and drug-likeness prediction

The hit compounds' Adsorption, Distribution, Metabolism, Excretion, and Toxicity (ADMET) profile was predicted using the SwissADME web server (http://www.swissadme.ch/). Lipinski's rule of 5[33] and Veber's rules[34] were used to

predict the drug-likeness of the hit compounds. Furthermore, the QikProp tools of the Schrodinger v12.4 were used to verify the outcome of the ADMET prediction from the SwissAMDE webserver; hence, compounds with high attrition during clinical screening can be eliminated before the trials.

In silico, validation of docking program

The validation of the docking program was performed to estimate the reliability of the docking simulation. The validation was performed in 2 ways. First, the program's accuracy measurement to predict the active site of the apo-protein crystal structure of HPA (ie, without the co-crystallized ligands—Montbretin A analog) was highlighted in Supplementary Tables 1 and 3. Second, the co-crystalized ligand was docked onto the apo-protein, and the root mean square deviation (RMSD) of the docked pose and the crystal structure pose of the co-crystallized (Montbretin A analog) was measured (Supplementary Figure 2). The docking program was excellent for the study as the RMSD was 0.1609 Å between the docked pose and the crystal structure pose. An RMSD below 2 Å is excellent for docking.[35]

Validation of the in silico docking results through accessing the in vitro alpha-amylase and alpha-glucosidase inhibitory activities of EELH

Alpha-glucosidase inhibition. Alpha-amylase inhibitory activity was determined using the method described by Kwon et al.[36] Variable concentrations (62-1000 µg/mL) of the extract were prepared and mixed with 500 µL of sodium phosphate buffer and 0.50 mg/mL of pancreatic alpha-amylase. The resulting mixture was incubated for 5 minutes at 37°C before adding 500 µL of starch solution. Further incubation was carried out in the water for 5 minutes at 37°C before adding 1.0 mL of dinitrosalicylic acid to stop the reaction. The control (reference sample) contains all the reagents except the starch solution. The absorbance of the cooled mixture was recorded at 540 nm using a spectrophotometer. All tests were performed in triplicate. Alpha-amylase inhibitory activity was calculated with the equation below

$$\text{Alpha-amylase inhibition } (\%) = \frac{absorbance\ of\ control - Absorbance\ of\ sample}{absorbance\ of\ control} \times 100$$

Alpha-glucosidase inhibition. Alpha-glucosidase inhibition by the plant extract (10-40 µg/mL) was measured according to the method of Matsui et al.[37] This was done by the determination of reducing sugar evolved from the hydrolysis of sucrose by alpha-glucosidase (Sigma-Aldrich, St. Louis, USA). All tests were performed in triplicate. The percentage of inhibition was calculated from the equation below

$$\text{Alpha-glucosidase inhibition } (\%) = \frac{Absorbance\ of\ control - Absorbance\ of\ sample}{Absorbance\ of\ control} \times 100$$

Statistical analysis

The IBM Statistical Package for Social Sciences (SPSS) (SPSS Inc, Chicago, IL, USA) was used to analyze the data obtained in this study. The values were analyzed descriptively and compared with the Duncan multiple tests using 1-way analysis of variance (ANOVA) and post hoc multiple comparisons. A *P*-value of less than .05 was assigned as the least significant threshold, and results were reported as mean ± SD. Half maximal inhibitory concentration (IC_{50}) and R^2 values were computed from the non-regression equation using GraphPad Prism version 6.5 (GraphPad Software, Inc, California, USA).

Results

Qualitative phytochemical screening of EELH

The result of qualitative phytochemical screening shows that EELH has a high concentration of flavonoids with moderate amounts of alkaloids and cardiac glycosides. Saponins, tannins, and steroids were present in low amounts, while terpenoids were not detected (Table 1).

Concentrations of vitamins and minerals present in L hastata leaf

The concentrations of vitamins present in the extract are 1.800 ± 0.32, 28.370 ± 2.451, and 0.600 ± 0.119 mg/100 g for vitamins A, C, and E, respectively, (Figure 1A) while minerals in their decreasing order are Ca > Fe > Mn > Zn > Cu (Figure 1B).

GC-MS profiling of EELH

The GC-MS analysis identified 32 phyto-chemotypes presented in Figure 2A (chromatogram) and Table 2, containing RT, area, molecular weight, formulae, and structures of the identified compounds. The compounds are the following: cyclooctane,2,4-Dinitro-1,3-dimethyl-benzeneBenzoicacid,2-Pyrrolidinone, triacetin, 1,2,3-Benzenetriol, 1,2-Benzenediol, acetophenone, benzoic acid, vanillic acid, triethyl citrate,

Table 1. Phytochemical screening of the EELH leaves.

PHYTOCHEMICAL	OBSERVATION	INFERENCE	REMARK
Alkaloids	Reddish-brown ppt	++	Moderate
Flavonoid	Yellow ppt	+++	High
Tannins	Light green	+	Low
Saponin	Light emulsion	+	Low
Cardiac glycoside	Brown color	++	Moderate
Terpenoids	Colorless	–	Absence
Steroids	Light brown	+	Low

+, ++, and +++ denote low, moderate, and high concentrations, respectively.

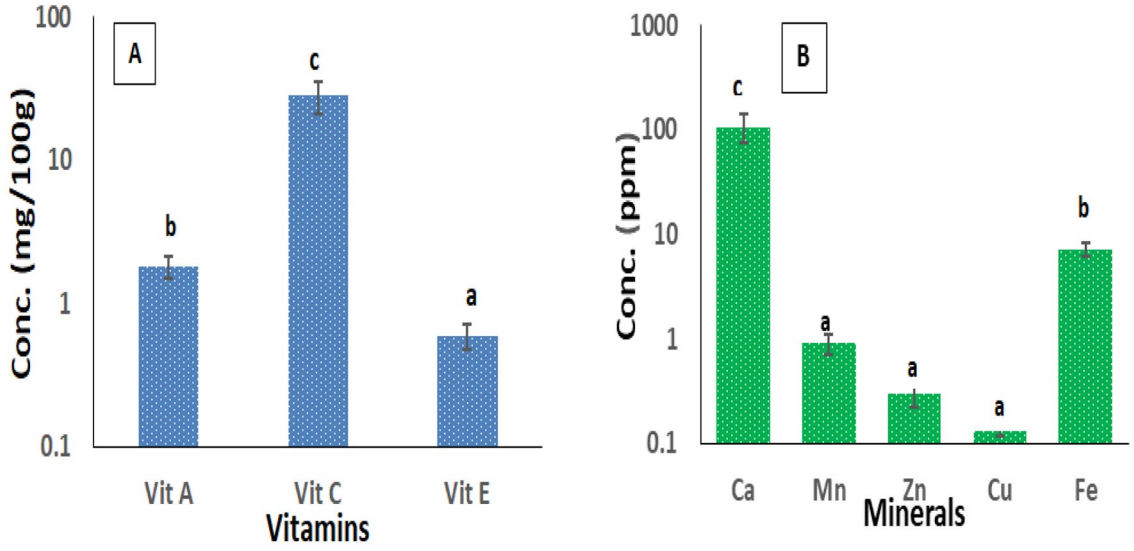

Figure 1. Antioxidant vitamins (A) and minerals (B) composition of EELH.
Values are presented as mean ± SD of triplicate determination. Mean values with different letters of alphabet differed from each other significantly at $P < .5$.
EELH indicates ethanol extract of *L hastata*.

pyrazole-5-carboxylic acid, propanoyl chloride, phthalic acid, n-Hexadecanoic acid, dibutyl phthalate, IH-Imidazole-4,5-dicarboxylic acid, diisooctyl phthalate, 5-Amino-2H-pyrazole-3-carboxamide, 5-Acetoxymethyl-2-furaldehyde, IH-3a, benzene, Trans-3-Undecene-1,5-diyne,3-Isopropyl-5-(phenoxymethyl)-2-oxazolidinone, 1-Octyl-2-(6-(4), 1-Docosene, Trans-3-Undecene-1,5-diyne, s-triazole-3-carboxaldehyde, 1-octyl-2-(6-(cyclopropane, Methyl 4-(2,4-dinitrophenylhydrazono) valerate, 2-Heptanol, 1-Methyl-2-benzylimino-1,2-dihydro-quinoline, and Silane.

Compounds identified from EELH using GC-FID

GC-FID screening of EELH identified a high concentration of sapogenin, catechin, steroids, cyanogenic glycosides, kaempferol, phytate, epicatechin, flavanones, phenols, sparteine, and naringenin. Moderate amounts of anthocyanin, ephedrine, cardiac glycosides, naringin, lunamarine, and rutin were recorded (Figure 2B and Table 3).

Quality of the preprocessed crystal protein structure and ligands, and validation of docking program

The quality of the prepared crystal structure of the protein was accessed using the Ramachandran plots (Supplementary Figure 1a) and the protein reliability report (Supplementary Figure 1b). The prepared structure was of good quality as there were no Ramachandran outliers, but only a few glycine residues (which do not significantly affect the structures) were dispersed. The prepared structure had no missing loops, no bond angle deviation, no unusual B-factor, and excellent protein packing (Supplementary Figure 1a and b). The buried unsatisfied donor and acceptor, and the peptide planarity, were not of significant concern (Supplementary Figure 1b). Other qualities, such as the noisy water molecules, were completely removed, and the overall structure of the crystal structure of HPA (6OCN) was completely energy-minimized (Supplementary Figure 1c and d).

Furthermore, the validation of the docking program was accessed to check for its suitability for the study. The

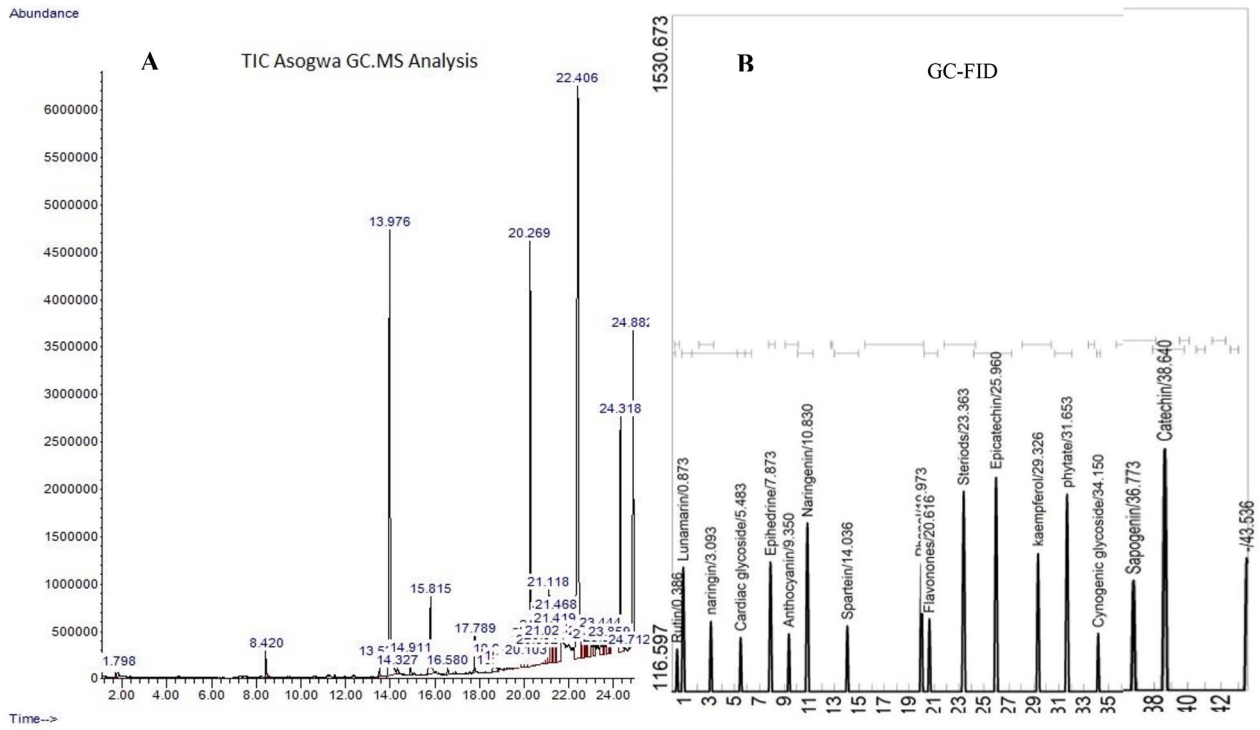

Figure 2. Chromatogram of different peaks identified in EELH using (A) GC-MS and (B) GC-FID.
GC-FID indicates gas chromatography–flame ionization detector; GC-MS, gas chromatography–mass spectrophotometer.

co-crystallized ligand was docked onto the apo-protein, and the RMSD of the docked pose and the crystal structure pose of the co-crystallized (Montbretin A analog) after superimposition was measured (Supplementary Figure 2). The docking program was excellent for the study as the RMSD was 0.1609 Å between the docked pose and the crystal structure pose. An RMSD below 2 Å is excellent for docking.[35]

E-pharmacophore model

The e-pharmacophore model generated from the complex of acarbose and the crystallized apo-protein was presented in Figure 3 (Supplementary Table 3), and its properties were summarized in Supplementary Table 1. The pharmacophore model had 5 features (ADDDD), comprising 4 hydrogen donor features and 1 hydrogen acceptor feature. The generated pharmacophore hypothesis was used to screen the ligand library comprising about 43 phytochemical constituents of the EELH. The selected compound must have at least 3 out of 5 features, an alignment score of at least 0.8, and a fitness score of at least 0.5. A total of 7 phytochemicals listed in Table 4 were selected for further molecular docking studies and ADMET screening.

Molecular docking

Molecular docking was used to predict the best energy-minimizing orientation of the phytochemicals in the active site of the HPA. Docking scores were assigned to the orientation of each ligand in the active site to indicate the strength of their affinities (the higher the negative value, the stronger the affinity). Based on the docking score and ligand efficiencies shown in Table 4, rutin, epicatechin, kaempferol, and naringenin were downstreamed for the ADMET analysis, and their interactions within the active site were analyzed and presented in both 3D (Figure 4) and 2D. (Figure 5) Rutin had hydrogen bond interactions with hydrophobic TYR 151, negatively charged ASP 300, polar HIS 305, and THR 163. Epicatechin established significant hydrogen bonds among polar HIS 201, positively charged LYS 200, and negatively charged ASP 197 using hydroxyl groups attached to the phenyl rings. Similarly, the phenyl ring of kaempferol interacted negatively with hydrophobic TRP59, while hydrogen bonds formed between negatively charged ASP 197, ASP 300, ASP 356, and HIS 305 via hydroxyl and carbonyl groups attached to the phenyl ring. The carbonyl group of naringenin established a significant hydrogen bond with polar THR 163 and negatively charged GLU 233. However, HIS 299 and LYS 200 amino acid residues used the hydroxyl groups on the HPA to form hydrogen bonds. The standard drug, acarbose, interacted with polar HIS 201, GLN 63, negatively charged LYS 200, GLU 240, GLU 220, ASP 300, and hydrophobic TRP 59. The top-scoring compounds also had favorable binding energy (Table 5).

ADMET properties

The results of ADMET screening predicted that among the top-scoring compounds, epicatechin, kaempferol, and naringenin had

Table 2. GC-MS profiling of volatile compounds in EELH.

S/N	COMPOUNDS	RT	AREA	MOL. WEIGHT, (G/MOL)	FORMULAE
1	Cyclooctane	1.688	0.05	112.21	C8H16
2	2,4-Dinitro-1,3-dimethyl-benzene Benzoic acid	1.798	0.26	172.58	C7H4N2O6
3	2-Pyrrolidinone	8.420	0.65	85.11	C4H7NO
4	Triacetin	13.529	0.35	218.21	C9H14O6
5	1,2,3-Benzenetriol	322.785	24.74	126.11	C6H6O3
6	1,2-Benzenediol	14.327	0.19	110.11	C6H6O2
7	Acetophenone	14.911	0.52	120.15	C6H5COCH3
8	Benzoic acid	34.481	4.20	122.12	C6H5COOH
9	Vanillic acid	16.580	0.19	168.14	C8H8O4
10	Triethyl citrate	17.789	0.70	176.283	$C_{12}H_{20}O_7$
11	Pyrazole-5-carboxylic acid	38.912	0.94	162.09	C5H4F2N2O2
12	Propanoyl chloride	19.159	0.29	92.52	C3H5ClO
13	Phthalic acid	20.269	12.47	166.14	C8H6O4
14	n-Hexadecanoic acid	21.118	2.52	256.4	$C_{16}H_{32}O_2$
15	Dibutyl phthalate	21.275	1.50	278.34	$C_{16}H_{22}O_4$
16	IH-Imidazole-4,5-dicarboxylic acid	21.468	3.47	156.10	C5H4N2O4
17	Diisooctyl phthalate	22.406	25.81	390.5561	$C_{24}H_{38}O_4$
18	5-Amino-2H-pyrazole-3-carboxamide	22.538	0.43	169.18	C7H11N3O2
19	5-Acetoxymethyl-2-furaldehyde	22.591	0.39	168.1467	C8H8O4
20	IH-3a	22.638	0.56	142.20	$C_{11}H_{10}$
21	Benzene	22.695	0.67	78.11	C6H6
22	Trans-3-Undecene-1,5-diyne	22.807	0.69	146.23	$C_{11}H_{14}$
23	3-Isopropyl-5-(phenoxymethyl)-2-oxazolidinone	22.919	0.95	129.1570	C6H11NO2
24	1-Octyl-2-(6-(4)	23.138	0.49	292.5	$C_{19}H_{32}O_2$
25	1-Docosene	23.444	0.80	308.6	$C_{22}H_{44}$
26	Trans-3-Undecene-1,5-diyne	47.326	0.95	146.23	$C_{11}H_{14}$
27	s-triazole-3-carboxaldehyde	23.806	0.17	97.08	C3H3N3O
28	1-octyl-2-(6-[hexyl] cyclopropane	23.841	0.16	126.24	C9H18
29	Methyl 4-(2,4-dinitrophenylhydrazono) valerate	23.859	0.38	130.18	C7H14O2
30	2-Heptanol	24.318	7.01	116.201	C7H16O
31	1-Methyl-2-benzylimino-1,2-dihydroquinoline	24.712	0.02	145.20	C8H8N2O
32	Silane	24.882	7.68	32.12	H4Si

Abbreviation: RT, retention time.

zero violations of both Lipinski and Veber rules for available oral drugs and a favorable bioavailability score of 0.55 in addition to a high gastrointestinal absorption (GIA). None of the screened compounds was brain-permeant. Among the screened compounds, rutin and epicatechin did not inhibit any isoforms, while kaempferol and naringenin inhibited CYP1A2 and CYP3A4 isoforms. None of the compounds will likely be hepatotoxic, mutagenic, or carcinogenic (Table 6).

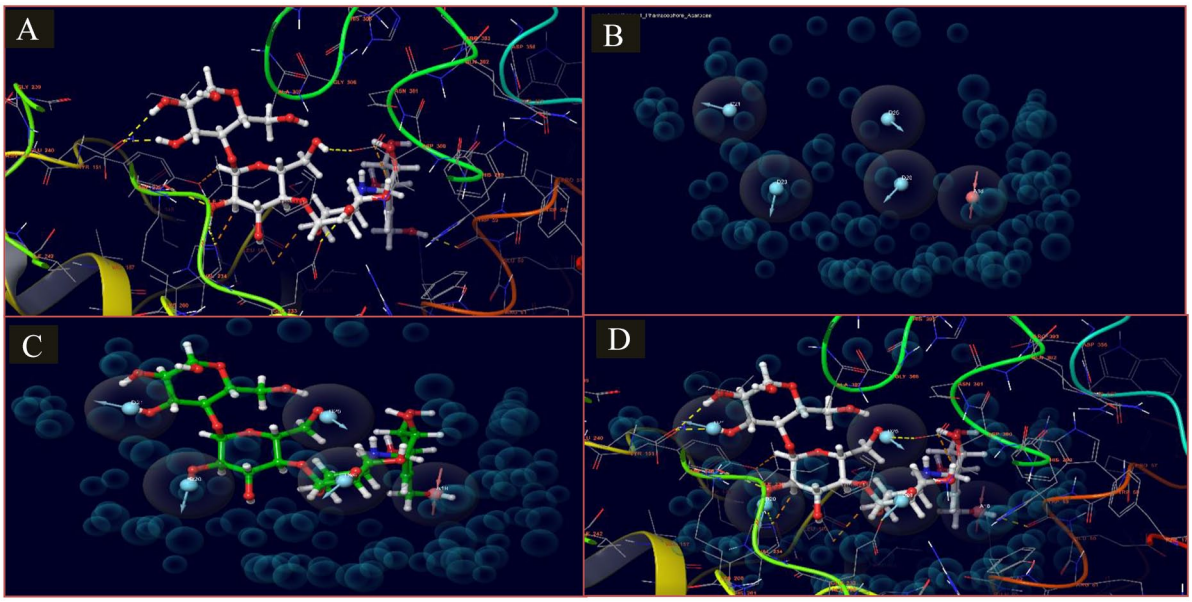

Figure 3. E-pharmacophore model of the IFD docked complex of acarbose and apo crystal structure of HPA (6OCN_A). (A) This shows the 3D representation of the docked complex and the interaction of acarbose atoms in the active site of HPA (6OCN_A). (B) The generated e-pharmacophore model is based on the stabilized and energy-minimized interaction in the complex. (C) Pharmacophore model on the interacting atoms of acarbose. (D) Pharmacophore model in the protein complex of acarbose and HPA (6OCN_A).
HPA indicates human pancreatic amylase; IFD, induced-fit docking.

Table 3. Non-volatile compounds identified with GC-FID in EELH.

S/N	COMPOUNDS	RT	AREA	MOL. WEIGHT, (G/MOL)	FORMULA	CLASS OF COMPOUNDS
1	Rutin	0.386	2631.04	610.521	$C_{27}H_{30}O_{16}$	Flavonoid
2	Lunamarine	0.873	4824.98	469.311	$C_{18}H_{15}NO_{14}$	Glycoside
3	Naringin	3.093	3389.30	580.53	$C_{27}H_{32}O_{14}$	Flavonoid
4	Cardiac glycosides	5.483	2954.84	780.9	$C_{14}H_{64}O_{13}$	Steroid
5	Ephedrine	7.873	2954.84	165.236	C10H15NO	Alkaloid
6	Anthocyanin	9.350	3057.12	1730.5	$C_{78}H_{89}O_{44}$	Flavonoid
7	Naringenin	10.830	6003.07	272.25	$C_{15}H_{12}O_5$	Flavonoid
8	Sparteine	14.036	3250.66	234.38	$C_{15}H_{26}N_2$	Alkaloid
9	Phenol	19.973	4928.68	94.11	C6H5OH	Phenol
10	Flavanones	20.616	3419.69	222.24	$C_{15}H_{10}O_2$	Flavonoid
11	Steroids	36.363	6954.48	358.4	$C_{19}H_{28}O_2$	Steroid
12	Epicatechin	25.960	7289.28	290.27	$C_{15}H_{14}O_6$	Flavonoid
13	Kaempferol	29.326	5273.28	286.23	$C_{15}H_{10}O_6$	Flavonoid
14	Phytate	31.653	6802.67	660.04	$C_6H_{18}O_{24}P_6$	Steroid
15	Cyanogenic glycoside	34.150	3084.59	247.24	C10H17NO6	Glycoside
16	Sapogenin	36.773	4449.93	1031.18	$C_{51}H_{82}O_{21}$	Saponin
17	Catechin	36.640	8024.05	290.26	$C_{15}H_{14}O_6$	Flavonoid

Abbreviations: GC-FID, gas chromatography–flame ionization detector; RT, retention time.

Table 4. Selected compounds screened from the EELH phytochemical libraries using the pharmacophore hypothesis (blue shade) and their docking score and ligand efficiencies (green shade).

SCREENED COMPOUNDS	NUMBER SITES MATCHED	MATCHED LIGAND SITES	ALIGN SCORE/ VECTOR SCORE	FITNESS	GLIDE ROTATABLE BONDS	DOCKING SCORE	XP GSCORE	GLIDE EVDW	GLIDE ENERGY
Rutin	5/5	A(14) D(25) D(26) D(21) D(23)	1.51/0.154	0.516	16	−10.517	−10.545	−39.294	−56.721
Epicatechin	4/5	A(-) D(10) D(9) D(11) D(8)	0.96/0.65	1.119	6	−7.398	−7.398	−25.501	−41.799
Kaempferol	3/5	A(-) D(7) D(8) D(9) D(-)	0.977/0.727	1.185	5	−7.031	−7.031	−26.454	−36.163
Cardiac glycoside	5/5	A(5) D(18) D(19) D(16) D(13)	1.397/0.477	0.685	12	−6.495	−6.495	−31.144	−42.945
Naringenin	3/5	A(-) D(-) D(8) D(6) D(7)	0.848/0.743	1.179	4	−6.413	−6.413	−27.668	−39.632
Sapogenin A	4/5	A(-) D(7) D(8) D(9) D(6)	1.826/0.571	0.531	6	−4.284	−4.284	−28.773	−33.787
5-Amino-2H-pyrazole-3-carboxamide	3/5	A(-) D(3) D(4) D(6) D(-)	0.887	0.992	1	−2.97	−2.97	−17.543	−19.442

Abbreviations: XP, extra precision; G score, glide score; evdw, electrostatic and Van der waals energy.

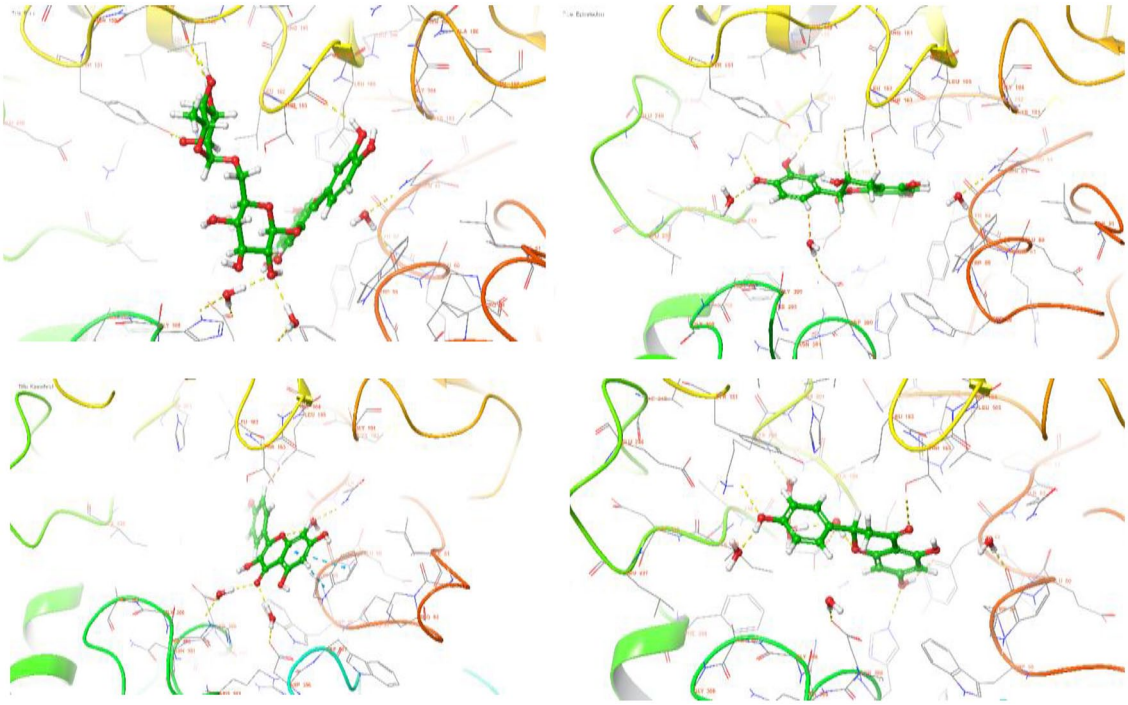

Figure 4. 3D representation of molecular docking poses of selected hit compounds from the extract of *L hastata*.

In vitro α-amylase and α-glucosidase inhibition

The result in Figure 6A shows that the extract inhibited α-amylase in a non-concentration-dependent manner, with a maximal inhibition of 61.91 ± 2.68 recorded at 1000 µg/mL. However, α-glucosidase enzyme activity inhibited concentration-dependent (Figure 6B). Inhibition of both enzymes had a very strong positive correlation with concentration (positive R^2 values), but α-amylase was less inhibited than α-glucosidase as revealed by their IC_{50} values of 14.14 and 4.22 µg/mL, respectively (Figure 6).

Discussion

Plants are endowed with phytochemicals such as alkaloids, flavonoids, steroids, saponins, and tannins that play a vital role in preventing and managing hyperglycemia.[2,13,16,17,38] Alkaloids, aromatic heterocyclic compounds containing nitrogen as a hetero atom, are employed as pharmaceutical agents to treat neurological disorders, cancer, and DM.[27] The anti-DM activities of alkaloids vary from the inhibition of carbohydrate digestive enzymes, improvement of insulin sensitivity and secretion, glucose uptake, and regulation of gene expression.[39] Phenolic compounds (flavonoids, phenols, and tannins) detected in the plant are potent antioxidants that ameliorate the onset of long-term diseases, including DM. The biochemical mechanisms of their action span from scavenging radicals, stimulation of the transcription factor Nrf2 required to protect cells against oxidative damage, to regulation of mediators and cell signaling pathways.[19] More strikingly, dietary flavonoids prevent DM and its associated complications by regulating glucose metabolism, scavenging free radicals and reactive species, and moderating hepatic enzyme activities and the lipid profile.[40] Also, tannins have an insulin-like impact on insulin-sensitive tissues, decreasing glucose levels by modulating the oxidative environment of pancreatic cells, delaying intestinal glucose absorption, and the onset of insulin-dependent DM.[40] Remarkably, studies have established a positive relationship between phenolic compounds and antidiabetic activity.[16] The presence of these anti-DM phytoconstituents in *L hastata* offers excellent therapeutic benefits.

The pathophysiology of DM has been linked to oxidative stress either as a causative factor or because of its consequences.[2] The detrimental effects of oxidative stress in long-term diseases such as DM could be inhibited by dietary antioxidants, such as vitamins and minerals.[10] Herein, substantial amounts of vitamins A, C, and E were identified. Vitamin A is a fat-soluble vitamin that acts as an antioxidant, regulator of endocrine development and pancreatic function.[41] The mechanisms of its antioxidant and antidiabetic action are chelation of oxygen radicals, increasing insulin sensitivity, and beta-cell regeneration.[41] It increases insulin secretion by activating the glucokinase promoter, which raises pancreatic glucokinase and regulates overexpression of uncoupling protein 1 (UCP-1), thereby averting insulin resistance.[42] Vitamin C disrupts free radical chain reactions and improves C-reactive proteins, lipid profiles, serum homocysteine, and incidence of DM[10] due to their influence on glucose metabolism. Thus, vitamin C supplements lower blood glucose and increase superoxide dismutase and glutathione level.[10] Similarly, supplementing vitamin E to DM patients is essential for restoring their antioxidant status and glycemic control. The physiological benefits of vitamin E could be anchored on its radical

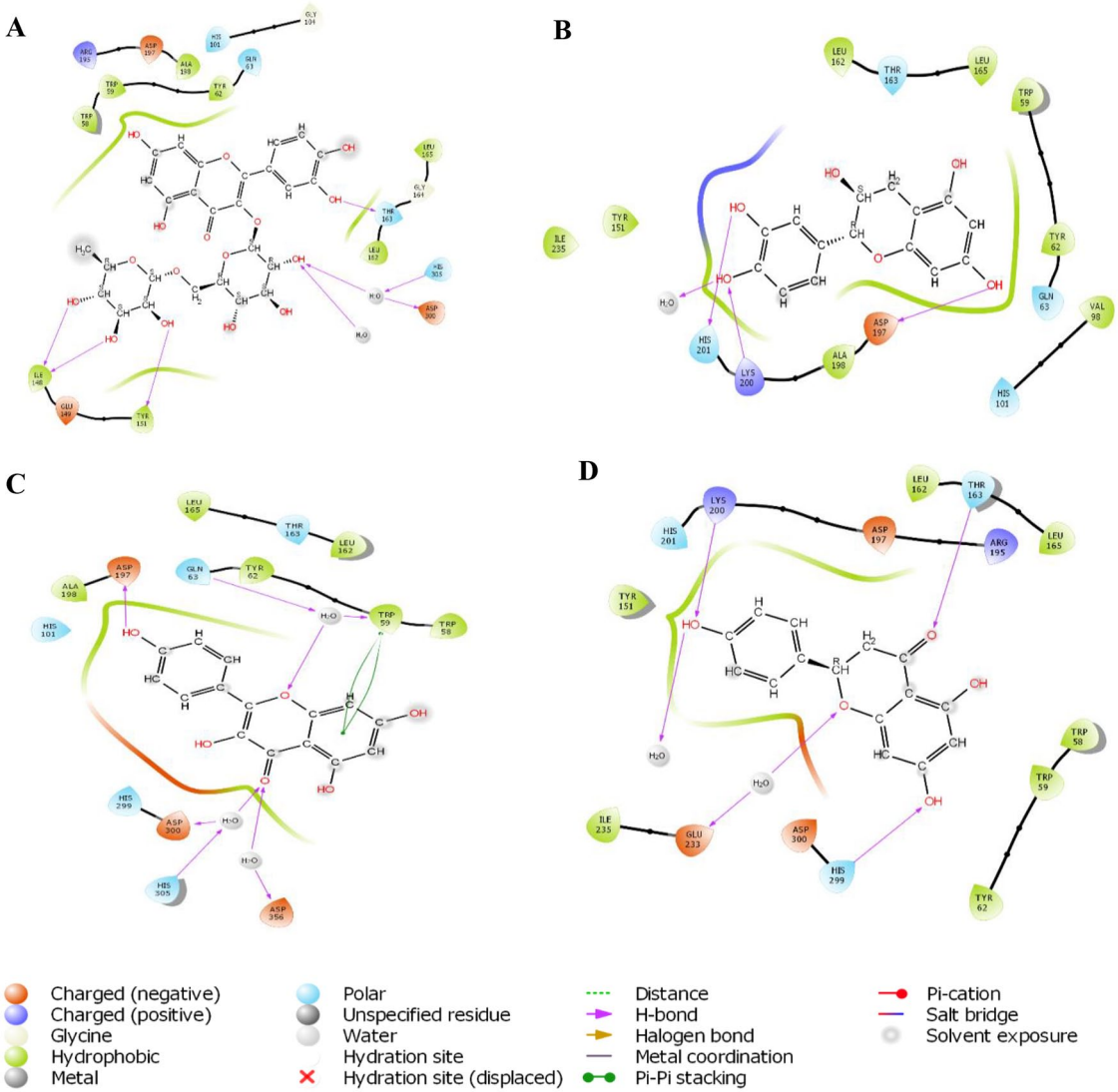

Figure 5. 2D representation of molecular docking poses of selected hit compounds from the extract of *L hastata* (rutin [A], epicatechin [B], kaempferol [C], naringenin [D]).

Table 5. Binding free energy calculated with MM-GBSA approach.

COMPOUNDS	ΔG_{BIND} (KCAL/MOL)	ΔG_{BIND} COULOMB	ΔG_{BIND} H-BOND	ΔG_{BIND} LIPOPHILIC	ΔG_{BIND} VDW	ΔG_{BIND} COVALENT
Rutin	−37.19	−54.62	−5.43	−10.14	−35.75	6.31
Epicatechin	−28.49	−41.16	−4.5	−9.76	−25.39	3.38
Kaempferol	−32.36	−20.22	−3.58	−9.45	−27.52	1.26
Naringenin	−29.6	−30.43	−2.6	−6.4	−28.61	1.93
Acarbose	−67.10	−41.45	−7.45	−22.53	−55.50	6.25

Abbreviation: MM-GBSA, molecular mechanics–generalized Born surface area.

scavenging effects, which help maintain functional and structural components of vessel and cell walls.[10] Overall, daily intake of vitamins prevents or delays the transition from pre-diabetes to T2D by improving pancreatic b-cell function. In light of this, the presence of these minerals and vitamins in *L hastata* could also be responsible for its anti-diabetic potency.

Furthermore, minerals and trace elements recorded in the plant (Ca, Mn, Zn, and Fe) are required as cellular materials for many metabolic activities inside the body, as cofactors for many

Table 6. ADMET prediction output of test compounds.

PARAMETERS	RUTIN	EPICATECHIN	KAEMPFEROL	NARINGENIN	ACARBOSE
Drug-likeness					
Mol. weight (g/mol)	610.52	290.3	286.24	272.3	645.60 g/mol
# Rotatable bonds	6	1	1	1	9
iLog P	2.43	1.47	1.70	1.75	0.63
# H-bond acceptor	16	6	6	5	19
# H-bond donor	10	5	4	3	14
Molar reactivity	141.38	74.33	76.01	71.57	136.69
TPSA (A^2)	269.43	110.4	111.13	86.99	321.17 A^2
Lipinski violations	3	0	0	0	3
Veber violations	1	0	0	0	1
Bioavailability score	0.17	0.55	0.55	0.55	0.17
Pharmacokinetics					
GI absorption	Low	High	High	High	Low
BBB permeant	No	No	No	No	No
P-gp substrate	Yes	Yes	No	Yes	Yes
CYP1A2 inhibitor	No	No	Yes	Yes	No
CYP2C19 inhibitor	No	No	No	No	No
CYP2C9 inhibitor	No	No	No	No	No
CYP2D6 inhibitor	No	No	Yes	No	No
CYP3A4 inhibitor	No	No	Yes	Yes	No
Log K_p (cm/s) (skin permeation)	–10.26	–7.82	–6.70	–6.17	–16.29 cm/s
Toxicity					
Predicted LD_{50} (mg/kg)	5000	10000	3919	2000	24000
Predicted toxicity class	5	6	5	4	6
Hepatotoxicity	–	–	–	–	+
Carcinogenicity	–	–	–	–	–
Immunogenicity	+	–	–	–	+
Mutagenicity	–	–	–	–	–
Cytotoxicity	–	–	–	+	–

Abbreviation: ADMET, Adsorption, Distribution, Metabolism, Excretion, and Toxicity; BBB, blood brain barrier; GI, gastrointestinal; LD50, lethal dose 50; TPSA, topological polar surface area; P-gp, P-glycoprotein; CYP1A2, CYP2C19, CYP2C9, CYP2D6, CYP3A4, cytochrome P450 enzymes variants..

enzymes and as stabilizing components of enzymes and proteins.[43] In the viewpoint of DM, minerals and trace elements are essential for regulating insulin metabolism. For instance, maintaining calcium homeostasis helps in cell recognition in erythrocytes, platelets, and cardiac and skeletal muscles, promoting insulin secretion and action. Abnormal calcium regulation decreases the β-cell function, which could alter glucose homeostasis.[43] Studies have shown that zinc is required for optimal maturation of insulin secretory granules, facilitates insulin release, and increases the sensitivity of the tissues to insulin action and the functioning of pancreatic beta cells.[16,44] Zinc also inhibits cytokine-induced islet cell destruction, preventing diabetes progression by improving insulin synthesis, storage, and secretion by pancreatic tissues.[41] Besides, impaired metabolism of zinc upregulates microangiopathic complications in diabetic patients.[43] Moreso, ferritin, the storage form

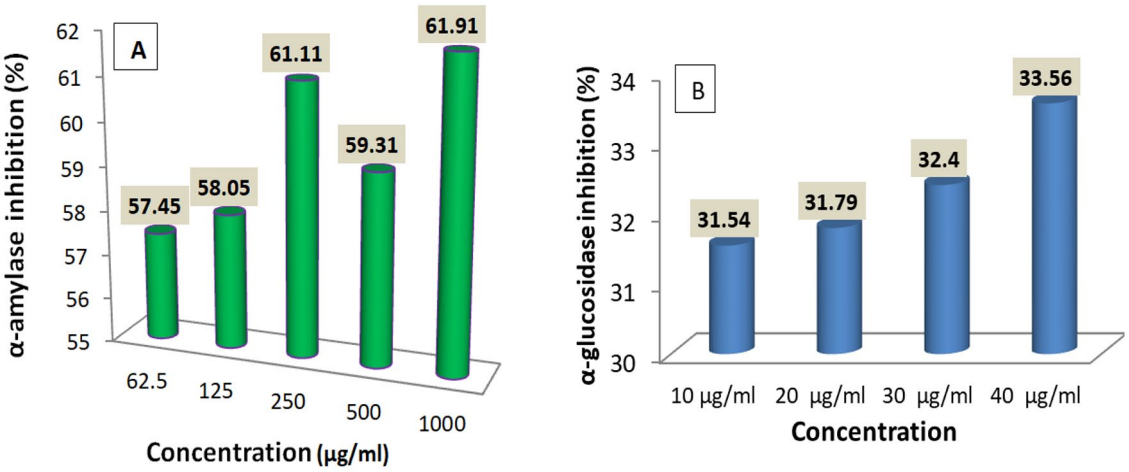

	IC_{50}	$Log\ IC_{50}$	R^2	Hill slope
α-amylase	14.14	1.150	0.9962	1.568
α-glucosidase	4.22	0.6252	0.9967	3.138

Figure 6. Effects of *L hastata* extract on α-amylase (A) and α-glucosidase (B) enzymes activities.

of iron, is an independent predictor in the glucose tolerance test because iron affects insulin sensitivity, vascular resistance, and oxidative damage.

The GC-MS screening identified 32 phyto-chemotypes, while the GC-FID results recorded a high abundance of alkaloids (lunamarine, ephedrine, and sparteine), phenols, flavonoids (rutin, naringenin, anthocyanin, epicatechin, kaempferol, and catechin), steroids, phytate, and saponin (sapogenin). Several compounds identified in the GC-MS and GC-FID data were found active in terms of anti-diabetic and antioxidant potential, as evident from their literature. Among these compounds, naringenin, rutin, catechin, kaempferol, epicatechin, and anthocyanin are powerful antioxidants and hypoglycemic agents.[45] Naringenin inhibits hyperglycemia by reducing renal glucose reabsorption, absorption of glucose by the intestinal brush border, and increasing glucose uptake and utilization by fat and muscle tissues.[46] Rutin regulates hyperglycemia by increasing glucose uptake in the peripheral tissue, suppressing gluconeogenesis in the liver, and stimulating insulin secretion and release.[42] The anti-DM effects of rutin could also be linked to its strong antioxidant and anti-inflammatory activities.[47] Almost similarly, catechin exerts anti-diabetic effects by boosting antioxidant status and could ameliorate diabetic autonomic nephropathy.[48] Reports have shown that kaempferol inhibits gluconeogenesis and enhances glucose metabolism.[49] The anti-diabetic activity of anthocyanidins is mainly by promoting insulin secretion and improving insulin resistance by reducing the levels of triacylglycerol, cholesterol, low-density lipoprotein, and apolipoprotein levels.[40] Thus, the therapeutic efficacy of *L hastata* could be anchored on these phytoconstituents.

Molecular docking is a veritable tool in drug discovery and development because of its uniqueness in determining the therapeutic efficacy of a drug with its target receptor or protein.[50] Thus, in silico and in vitro models provide an adequate basis for the potency of a drug target in experimental animals.[51] A favorable binding interaction occurred between HPA and the top-4 scoring compounds (rutin, epicatechin, kaempferol, and naringenin), almost similar to acarbose's standard drug. Enzyme kinetics studies and X-ray crystal structure of HPA revealed that the HPA active site is occupied by 3 essential amino acid residues, namely ASP 197, Glu 233, and ASP 300.[32] ASP 197 acts as a catalytic nucleophile in polymeric hydrolysis substrates such as starch. Glu 233 is used as an acid-base catalyst for substrate hydrolysis, while ASP 300 optimizes the orientation of the substrate.[3] The top-4 scoring compounds from *L hastata* interacted with these amino acid residues and other residues involved in HPA catalytic activity, suggesting mixed-type and non-competitive inhibition, as previously reported by Mazumdar et al.[13] Their interactions mainly were mediated by hydrogen bonds and stack interactions involving hydroxyl, carbonyl, and oxygen atoms attached to the phenyl rings. Hydrogen bonds play a vital role in the structural stability of biomolecules and enzyme stability. Stack interactions are the most appealing option among non-covalent interactions that play an essential role in the stability of ligand-protein complexes.[32] The phenyl ring in amino acids, such as tryptophan, histidine, tyrosine, and phenylalanine, is vital in drug design because it enhances molecular interactions, protein stability, and molecular recognition processes improving drug-like molecule specificity and binding energy.[52]

The binding energy algorithm validates results obtained in docking studies. Higher binding free energy denotes good and stable stability of the ligand-bound proteins. The major donors of the binding free energy are coulomb energy, covalent energy, hydrogen bonding, lipophilic bonding, and van der Waals energy.[4] Rutin, epicatechin, kaempferol, and naringenin

showed favorable binding energies of −37.19, −28.49, −32.36, and −29.6, respectively (Table 3). This strong binding energy establishes the stability of the compounds in the active sites of HPA because several studies have confirmed a significant correlation between MM-GBSA scoring and experimentally determined activity.[32,53] Moreover, the coulomb energy, the binding energy for hydrogen bonds, lipophilic groups, and van der Waals were also presented.

Drug-likeness is a medicinal property employed in drug discovery to predict the pharmacokinetics-related failure of drugs in clinical trials with high precision.[54,55] This study investigated the drug-likeness of the top-scoring compounds, taking into consideration the "Rule of 5" (RO5) (MW < 500, Log P ⩽ 5, HBA ⩽ 10, and HBD ⩽ 5) by Lipinski et al[33] in addition to Veber et al[34] rule of Not < 5 and TPSA ⩽ 140 A^2. Interestingly, all the compounds meet the RO5 and Veber rules, but rutin and their oral availability were also confirmed by their favorable bioavailability score (0.55%), which suggests that they are good oral drugs for the treatment of DM. However, acarbose violated Lipinski and Veber's rules, having an MW of 645.60 g/mol, 19 HBA, 14 HBD, 9 Nrot, and a TPSA value of 321.17 A^2, which may account for its undesirable side effects. Violation of Lipinski rule and lower bioavailability scores are indices that a compound is not likely to be orally active.[56] In addition, the high GI absorption by epicatechin, kaempferol, and naringenin indicates that they could be easily absorbed on oral administration. The high GIA of these compounds is of immense therapeutic benefit in DM because they are required to reduce postprandial glucose levels by inhibiting the activities of α-amylase and α-glucosidase in the gastrointestinal tract (GIT).[57] However, rutin with low GIA could work by other mechanisms and be administered via other routes such as para-cellular diffusion, passive, lipoidal diffusion, and uptake by transporter protein.[58] Importantly, rutin being a substrate to P-glycoprotein, an ATP-binding transmembrane glycoprotein responsible for active efflux of drugs and other chemicals out of the cells[57] suggests a promising hindrance of rutin toxicity elevation.

Cytochrome P450 isoenzymes family are needed for the first phase of biotransformation of xenobiotics and drugs in the liver. The isoenzymes CYP450 2C19 and CYP450 2C9 mediate drug plasma concentration, whereas CYP450 2D6 and CYP450 3A4 are required for the O-dealkylation reaction.[55] Rutin and epicatechin did not inhibit any of the isoforms. In contrast, kaempferol and naringenin inhibited some of the isoforms, suggesting that they are not likely to induce toxicity due to drug-drug interactions. This is in tandem with the predicted toxicity profile, which revealed that all the compounds are safe, having an LD_{50} ranging from 2000 to 10 000 mg/kg body, which is far above the doses usually prescribed for treatment. It is also worth noting that all the screened compounds are not likely to be hepatotoxic, mutagenic, or carcinogenic against the standard drug, acarbose, which is hepatotoxic.

PPHG is a significant biomarker of deregulated glucose homeostasis, which plays an essential role in T2D complications, such as cardiovascular, cerebrovascular, and neuropathy diseases.[59] Accordingly, the regulation of postprandial blood glucose is one of the most important therapeutic targets for DM treatment.[49] Its reduction using the inhibitors of α-amylase and α-glucosidase in T2D patients decreases glycated hemoglobin levels and prevents diabetic complications.[58] The results obtained in this study showed that *L hastata* extracts demonstrated the ability to reduce PPHG by inhibiting the activities of α-amylase and α-glucosidase. This potency could be a result of the synergistic effects of the bioactive compounds present in the leaf. Presumably, the high abundance of flavonoids and alkaloids, which are glucose-lowering agents,[39,60] and vitamins may account for the observed potential. Inhibition of these enzymes authenticates the anti-diabetic effects of the plant and confirms that it could serve as a drug target for DM.

Conclusions

The findings from this study show that *L hastata* leaves have higher flavonoids and an abundance of vitamin C and other bioactive compounds. The favorable interaction and binding energy of *L hastata* ligands to HPA suggest the therapeutic potential of the ligands against DM. Interestingly, the screened compounds also had favorable drug-like potency and safety profiles compared with the standard drug, acarbose. Furthermore, validation of the plant's efficacy as an anti-DM therapy using amylase and glucosidase inhibition models also authenticated the anti-diabetic effects of the plant. Hence, this study validates the use of *L hastata* as an anti-diabetic agent in folk medicine practice and brings the plant into the spotlight in searching for novel and safe anti-diabetic agents for drug development.

Author Contributions

IFC contributed to the conceptualization, investigation, data curation, resources, writing—critical review and editing, and supervision of the study. FNN and VOA contributed to the methodology, formal analysis, investigation, and writing—original draft. KOO contributed to the conceptualization, formal analysis, investigation, and methodology of the study. EJN contributed to the methodology, data curation, and writing—original draft. CDA contributed to the methodology, formal analysis, investigation, resources, and writing—original draft. TPCE contributed to the methodology, data curation, software, writing—original draft and editing of this study. All authors approved the final article before submission.

Ethical Approval

Not applicable to this study.

Supplemental Material

Supplemental material for this article is available online.

REFERENCES

1. Gupta A, Behl T, Sehgal A, et al. Unmasking the therapeutic potential of biomarkers in type-1 diabetes mellitus. *Biointerface Res Appl Chem*. 2021;11:13187-13201. doi:10.33263/BRIAC115.1318713201.
2. Oyetayo FL, Oseni OA, Akinlolu OS, Momodu DU. Antidiabetic, antilipidemic and antioxidant properties of aqueous extracts of *Morinda lucida* and *Nauclea latifolia* leaves in alloxan induced rats. *Biointerface Res Appl Chem*. 2021;11:11602-11615. doi:10.33263/BRIAC114.1160211615.
3. Alqahtani AS, Hidayathulla S, Rehman MT, et al. Alpha-amylase and alpha-glucosidase enzyme inhibition and antioxidant potential of 3-oxolupenal and katononic acid isolated from Nuxia oppositifolia. *Biomolecules*. 2020;10:61. doi:10.3390/biom10010061.
4. Ojo OA, Adegboyega AE, Johnson GI, et al. Deciphering the interactions of compounds from *Allium sativum* targeted towards identification of novel PTP 1B inhibitors in diabetes treatment: a computational approach. *Inform Med Unlocked*. 2021;26:100719. doi:10.1016/j.imu.2021.100719.
5. Tran N, Pham B, Le L. Bioactive compounds in anti-diabetic plants: from herbal medicine to modern drug discovery. *Biology (Basel)*. 2020;9:1-31. doi:10.3390/biology9090252.
6. Bhatia A, Singh B, Arora R, Arora S. In vitro evaluation of the α-glucosidase inhibitory potential of methanolic extracts of traditionally used antidiabetic plants. *BMC Complement Altern Med*. 2019;19:74. doi:10.1186/s12906-019-2482-z.
7. Yohanna FT, Haruna WC, Yerima TS, Sodipo OA, Falmata A. Phytochemical screening and antidiabetic effect of ethanol extracts of *Leptadenia hastata* plant (Pers.) Decne) in alloxan-induced diabetic rats. *Niger J Pharm Biomed Res*. 2018;3:22-27.
8. Thakral S, Narang R, Kumar M, Singh V. Synthesis, molecular docking and molecular dynamic simulation studies of 2-chloro-5-[(4-chlorophenyl) sulfamoyl]-N-(alkyl/aryl)-4-nitrobenzamide derivatives as antidiabetic agents. *BMC Chem*. 2020;14:49. doi:10.1186/s13065-020-00703-4.
9. Kumar V, Abbas A, Aster J. *Robbins & Cotran Pathologic Basis of Disease*. 10th ed. Amsterdam: Elsevier Health Science; 2021.
10. Balbi ME, Tonin FS, Mendes AM, et al. Antioxidant effects of vitamins in type 2 diabetes: a meta-analysis of randomized controlled trials. *Diabetol Metab Syndr*. 2018;10:18. doi:10.1186/s13098-018-0318-5.
11. Kabir N, Alhaji UI, James DB, Inuwa HM, Atiku MK. Effect of the combination of *Leptadenia hastata* (pers) decne and *Momordica balsamina* linn leaf extracts on lipid profile of streptozotocin-induced diabetic rats. *Futur J Pharm Sci*. 2021;7:110. doi:10.1186/s43094-021-00263-x.
12. Agu KC, Eluehike N, Ofeimun RO, et al. Possible anti-diabetic potentials of *Annona muricata* (soursop): inhibition of α-amylase and α-glucosidase activities. *Clin Phytoscience*. 2019;5:21. doi:10.1186/s40816-019-0116-0.
13. Mazumdar S, Marar T, Patki J, Devarajan S, Zambare V, Swami D. In silico and in vitro analysis reveal multi-target anti-hyperglycaemic properties of gedunin, a limonoid from neem (*Azadirachta indica*). *Clin Phytoscience*. 2020;6:25. doi:10.1186/s40816-020-00175-y.
14. Zheleva-Dimitrova D, Zengin G, Ak G, et al. Innovative biochemometric approach to the metabolite and biological profiling of the Balkan thistle (*Cirsium appendiculatum* Griseb.), Asteraceae. *Plants*. 2021;10:2046. doi:10.3390/plants10102046.
15. Thongnum K, Chanthai S. Inhibitory reactivity of capsaicin with α-amylase and α-glucosidase related to antidiabetes using molecular docking and quantum calculation methods. *Orient J Chem*. 2018;34:2211-2228. doi:10.13005/ojc/340501.
16. Al-omar MS, Mohammed HA, Mohammed SAA, et al. Anti-microbial, antioxidant, and α-amylase inhibitory activity of traditionally-used medicinal herbs : a comparative analyses of pharmacology, and phytoconstituents of regional halophytic plants' diaspora. *Molecules*. 2020;25:5457-5469. doi:doi:10.3390/molecules25225457.
17. Saidu Y, Muhammad SA, Abbas AY, Onu A, Tsado IM, Muhammad L. In vitro screening for protein tyrosine phosphatase 1B and dipeptidyl peptidase IV inhibitors from selected Nigerian medicinal plants. *J Intercult Ethnopharmacol*. 2017;6:154-157. doi:10.5455/jice.20161219011346.
18. Aouadi K, Hajlaoui H, Arraouadi S, Ghannay S, Snoussi M, Kadri A. Inhibitory potential of phenolic-enriched extracts of the aerial parts from *Echium humile* Desf.: in vitro combined with in silico approach. *Plants*. 2022;11:1131-1146. doi:10.3390/plants11091131.
19. Chukwuma IF, Nkwocha CC, Ezeanyika LUS, Ogugua VN. Phytochemical investigation and in vitro antioxidant potency of root bark of *Brenania brieyi* fractions. *Trop J Nat Prod Res*. 2020;4:970-975. doi:10.26538/tjnpr/v4i11.21.
20. Chukwuma IF, Apeh VO, Nwora FN, Nkwocha CC, Mba SE, Ossai EC. Phytochemical profiling and antioxidative potential of phenolic-rich extract of *Cola acuminata* nuts. *Biointerface Res Appl Chem*. 2023;13:29-39.
21. Okeke ES, Nweze EJ, Chibuogwu CC, Anaduaka EG, Chukwudozie KI, Ezeorba TPC. Aquatic phlorotannins and human health: bioavailability, toxicity, and future prospects. *Nat Prod Commun*. 2021;16:1934578X2110561. doi:10.1177/1934578X211056144.
22. Ezema CA, Ezeorba TPC, Aguchem RN, Okagu IU. Therapeutic benefits of Salvia species: a focus on cancer and viral infection. *Heliyon*. 2022;8:e08763. doi:10.1016/j.heliyon.2022.e08763.
23. Ezeorba TPC, Ezema CA, Asomadu RO, et al. Allistatin: a potent yet uncharacterized therapeutic nugget in *Allium sativum*. *Pharmacol Res Mod Chinese Med*. 2022;3:100121. doi:10.1016/J.PRMCM.2022.100121.
24. Galani BRT, Owona BA, Chuisseu DPD, Machewere E, Ngantchouko CBN, Moundipa PF. Hepatoprotective activity of *Leptadenia hastata* (*Asclepiadaceae*) on Acetaminophen-induced toxicity in mice: in vivo study and characterization of bioactive compounds through molecular docking approaches. *Biomed Res Int*. 2020;2020:3807234. doi:10.1155/2020/3807234.
25. Trease GE, Evans W. *Pharmacognosy*. 11th ed. London, England: Macmillan; 1989.
26. Harborne JB. *Phytochemicals Methods: A Guide to Modern Technique of Plant Analysis*. 2nd ed. New York, NY: Chapman and Hall; 1998.
27. Sarkar T, Salauddin M, Pati S, Sheikh HI. Application of raw and differently dried pineapple (*Ananas comosus*) pulp on rasgulla (sweetened *Casein Ball*) to enhance its phenolic profile, shelf life, and in-vitro digestibility characteristics. *J Food Process Preserv*. 2021;45:e15233. doi:10.1111/jfpp.15233.
28. AOVC. *Association of Vitamin Chemist: Methods of Vitamin Assay*. 3rd ed. New York, NY: John Wiley & Sons; 1966.
29. AOAC. *Official Methods of Analysis, Association of Official Analytical Chemist*. 19th ed. Arlington, VA: Association of Official Analytical Chemists; 2012.
30. Bezerra KS, Filho NRA. Characterization and quantification by gas chromatography of free steroids in unsaponifiable matter of vegetable oils. *J Braz Chem Soc*. 2014;25:238-245. doi:10.5935/0103-5053.20130288.
31. Tysoe CR, Caner S, Calvert MB, Win-Mason A, Brayer GD, Withers SG. Synthesis of montbretin A analogues yields potent competitive inhibitors of human pancreatic α-amylase. *Chem Sci*. 2019;10:11073-11077. doi:10.1039/C9SC02610J.
32. Kikiowo B, Ogunleye JA, Iwaloye O, Ijatuyi TT. Therapeutic potential of *Chromolaena odorata* phyto-constituents against human pancreatic α-amylase. *J Biomol Struct Dyn*. 2022;40:1801-1812. doi:10.1080/07391102.2020.1833758.
33. Lipinski CA, Lombardo F, Dominy BW, Feeney PJ. Experimental and computational approaches to estimate solubility and permeability in drug discovery and development settings. *Adv Drug Deliv Rev*. 2012;64:4-17. doi:10.1016/j.addr.2012.09.019.
34. Veber DF, Johnson SR, Cheng HY, Smith BR, Ward KW, Kopple KD. Molecular properties that influence the oral bioavailability of drug candidates. *J Med Chem*. 2002;45:2615-2623. doi:10.1021/jm020017n.
35. El-Kelawy HM, Mansour MA, El-Naggar RE, Nabila E, Elkassas EM. Effect of garlic (*Allium sativum*) treatment on hematological, biochemical, hormonal and fertility parameters of male BOUSCAT rabbits. *Egypt J Rabbit Sci*. 2017;27:341-358.
36. Kwon Y, Apostolidis E, Shetty K. α-amylase and α-glucosidase for management of hyperglycemia linked to type 2 diabetes. *J Food Biochem*. 2008;32:15-31.
37. Matsui T, Yoshimoto C, Osajima K, Oki T, Osajima Y. In vitro survey of α-glucosidase inhibitory food components. *Biosci Biotechnol Biochem*. 1996;60:2019-2022.
38. Ezeorba TPC, Chukwudozie KI, Ezema CA, Anaduaka EG, Nweze EJ, Okeke ES. Potentials for health and therapeutic benefits of garlic essential oils: recent findings and future prospects. *Pharmacol Res Mod Chinese Med*. 2022;3:100075. doi:10.1016/J.PRMCM.2022.100075.
39. Rasouli H, Yarani R, Pociot F, Popović-Djordjević J. Anti-diabetic potential of plant alkaloids: revisiting current findings and future perspectives. *Pharmacol Res*. 2020;155:104723. doi:10.1016/j.phrs.2020.104723.
40. Sun C, Zhao C, Guven EC, et al. Dietary polyphenols as antidiabetic agents: advances and opportunities. *Food Front*. 2020;1:18-44. doi:10.1002/fft2.15.
41. Said E, Mousa S, Fawzi M, Sabry NA, Farid S. Combined effect of high-dose vitamin A, vitamin E supplementation, and zinc on adult patients with diabetes: a randomized trial. *J Adv Res*. 2021;28:27-33. doi:10.1016/j.jare.2020.06.013.
42. Egbuna C, Awuchi CG, Kushwaha G, et al. Bioactive compounds effective against type 2 diabetes mellitus: a systematic review. *Curr Top Med Chem*. 2021;21:1067-1095. doi:10.2174/1568026621666210509161059.
43. Dubey P, Thakur V, Chattopadhyay M. Role of minerals and trace elements in diabetes and insulin resistance. *Nutrients*. 2020;12:1864. doi:10.3390/nu12061864.
44. Bharti SK, Krishnan S, Kumar A, Kumar A. Antidiabetic phytoconstituents and their mode of action on metabolic pathways. *Ther Adv Endocrinol Metab*. 2018;9:81-100. doi:10.1177/2042018818755019.
45. Ugoeze CK, Oluigbo EK, Chinko CBB. Phytomedicinal and nutraceutical benefits of the GC-FID quantified phytocomponents of the aqueous extract of *Azadirachta indica* leaves. *J Pharm Pharmacol Res*. 2020;4:149-163. doi:10.26502/fjppr.039.
46. Hartogh DD, Tsiani E. Antidiabetic properties of naringenin: a citrus fruit polyphenol. *Biomolecules*. 2019;9:99-119. doi:10.3390/biom9030099.
47. Nkwocha CC, Ogugofor MO, Chukwuma IF, Njoku OU. Identification and characterization of phytochemicals and constituents in *Desmodium velutinum*

stem using high-performance liquid chromatography (HPLC). *Pharmacol Res Mod Chinese Med*. 2022;3:100090. doi:10.1016/j.prmcm.2022.100090.
48. Hariftyani AS, Kurniawati LA, Khaerunnisa S, Veterini AS, Setiawati Y, Awaluddin R. In silico analysis of potential antidiabetic phytochemicals from Matricaria chamomilla L. against ptp1b and aldose reductase for type 2 diabetes mellitus and its complications. *Nat Prod Sci*. 2021;27:99-114. doi:10.20307/nps.2021.27.2.99.
49. Ojo OA, Oni AI, Grant S, et al. Antidiabetic activity of elephant grass (*Cenchrus purpureus* (Schumach.) Morrone) via activation of PI3K/AkT signaling pathway, oxidative stress inhibition, and apoptosis in Wistar rats. *Front Pharmacol*. 2022;13:845196. doi:10.3389/fphar.2022.845196.
50. Ezeorba TPC, Uchendu NO, Nweze EJ, et al. A probable anti-COVID phytochemical (1,7-bis-(4-hydroxyphenyl)-1-heptene-3,5-dione) screened computationally from the rhizome of curcuma longa. *Med Sci Forum*. 2021;7:6. doi:10.3390/ECMS2021-10845.
51. Mahnashi MH, Alqahtani YS, Alqarni AO, et al. Crude extract and isolated bioactive compounds from *Notholirion thomsonianum* (Royale) Stapf as multitargets antidiabetic agents: in-vitro and molecular docking approaches. *BMC Complement Med Ther*. 2021;21:1-13. doi:10.1186/s12906-021-03443-7.
52. Lanzarotti E, Defelipe LA, Marti MA, Turjanski AG. Aromatic clusters in protein-protein and protein-drug complexes. *J Cheminform*. 2020;12:1-9.
53. Maffucci I, Hu X, Fumagalli V, Contini A. An efficient implementation of the Nwat-MMGBSA method to rescore docking results in medium-throughput virtual screenings. *Front Chem*. 2018;6:43. doi:10.3389/FCHEM.2018.00043/BIBTEX.
54. Apeh VO, Njoku OU, Nwodo FOC, Chukwuma IF, Emmanuel AA. In silico drug-like properties prediction and in vivo antifungal potentials of *Citrullus lanatus* seed oil against *Candida albicans*. *Arab J Chem*. 2022;15:103578. doi:10.1016/j.arabjc.2021.103578.
55. Da Rocha MN, Marinho ES, Marinho MM, Dos Santos HS. Virtual screening in pharmacokinetics, bioactivity, and toxicity of the amburana cearensis secondary metabolites. *Biointerface Res Appl Chem*. 2022;12:8471-8491. doi:10.33263/BRIAC126.84718491.
56. Johnson TO, Adegboyega AE, Ojo OA, et al. A computational approach to elucidate the interactions of chemicals from Artemisia annua targeted toward SARS-CoV-2 main protease inhibition for COVID-19 treatment. *Front Med (Lausanne)*. 2022;9:907583. doi:10.3389/fmed.2022.907583.
57. Ononamadu CJ, Ibrahim A. Molecular docking and prediction of ADME/drug-likeness properties of potentially active antidiabetic compounds isolated from aqueous-methanol extracts of *Gymnema sylvestre* and *Combretum micranthum*. *BioTechnologia*. 2021;102:85-99. doi:10.5114/bta.2021.103765.
58. Harley BK, Kingsley B, Kingsley I, et al. *Myrianthus libericus*: possible mechanisms of hypoglycaemic action and in silico prediction of pharmacokinetics and toxicity profile of its bioactive metabolite, friedelan-3-one. *Biomed Pharmacother*. 2021;137:111379. doi:10.1016/j.biopha.2021.111379.
59. Amin E, Abdel-bakky MS, Darwish MA, et al. The glycemic control potential of some Amaranthaceae plants, with particular reference to in vivo antidiabetic potential of *Agathophora alopecuroides*. *Molecules*. 2022;27:973-983. doi:10.3390/molecules27030973.
60. Rajan M, Chandran V, Shahena S, Anie Y, Mathew L. In vitro and in silico inhibition of α-amylase, α-glucosidase, and aldose reductase by the leaf and callus extracts of *Vernonia anthelmintica* (L.) Willd. *Adv Tradit Med*. 2022;22:125-139. doi:10.1007/s13596-020-00533-8.